
11 Sep 2020

Mathematical Modeling and Pointwise Validation of a Spouted Bed using an Enhanced Bed Elasticity Approach

Sebastián Uribe

Binbin Qi

Omar Farid

Muthanna H. Al-Dahhan

Missouri University of Science and Technology, aldahhanm@mst.edu

Follow this and additional works at: https://scholarsmine.mst.edu/che_bioeng_facwork

 Part of the [Chemical Engineering Commons](#)

Recommended Citation

S. Uribe et al., "Mathematical Modeling and Pointwise Validation of a Spouted Bed using an Enhanced Bed Elasticity Approach," *Energies*, vol. 13, no. 18, MDPI, Sep 2020.

The definitive version is available at <https://doi.org/10.3390/en13184738>



This work is licensed under a [Creative Commons Attribution 4.0 License](#).

This Article - Journal is brought to you for free and open access by Scholars' Mine. It has been accepted for inclusion in Chemical and Biochemical Engineering Faculty Research & Creative Works by an authorized administrator of Scholars' Mine. This work is protected by U. S. Copyright Law. Unauthorized use including reproduction for redistribution requires the permission of the copyright holder. For more information, please contact scholarsmine@mst.edu.

Article

Mathematical Modeling and Pointwise Validation of a Spouted Bed Using an Enhanced Bed Elasticity Approach

Sebastián Uribe ¹ , Binbin Qi ¹, Omar Farid ¹ and Muthanna Al-Dahhan ^{1,2,*}

¹ Chemical and Biochemical Engineering Department, Missouri University of Science and Technology, Rolla, MO 65409, USA; uribelopezj@mst.edu (S.U.); bq6vf@mst.edu (B.Q.); ogy4h5@mst.edu (O.F.)

² Mining and Nuclear Engineering Department, Missouri University of Science and Technology, Rolla, MO 65409, USA

* Correspondence: aldahhanm@mst.edu

Received: 10 August 2020; Accepted: 9 September 2020; Published: 11 September 2020



Abstract: With a Euler–Euler (E2P) approach, a mathematical model for predicting the pointwise hydrodynamic behavior of a spouted bed was implemented through computational fluid dynamics (CFD) techniques. The model considered a bed elasticity approach in order to reduce the number of required sub-models to provide closure for the solids stress strain-tensor. However, no modulus of elasticity sub-model for a bed elasticity approach has been developed for spouted beds, and thus, large deviations in the predictions are obtained with common sub-models reported in literature. To overcome such a limitation, a new modulus of elasticity based on a sensitivity analysis was developed and implemented on the E2P model. The model predictions were locally validated against experimental measurements obtained in previous studies. The experimental studies were conducted using our in-house developed advanced γ -ray computed tomography (CT) technique, which allows to obtain the cross-sectional time-averaged solids holdup distribution. When comparing the model predictions against the experimental measurements, a high predictive quality for the radial solids holdup distribution in the spout and annulus regions is observed. The model predicts most of the experimental measurements for different particle diameters, different static bed heights, and different inlet velocities with deviations under 15%, with average absolute relative errors (AARE) between 5.75% and 7.26%, and mean squared deviations (MSD) between 0.11% and 0.24%

Keywords: spouted bed; CFD modeling; Euler-two-phase model; elasticity modulus; validation experiments

1. Introduction

Since the early development of spouted beds in 1954 [1,2], these gas–solid contactors have been widely used for several industrial applications—such as fast catalytic reactions, gasification, catalytic polymerization, pyrolysis, coating, drying, and granulation [3–7]—due to their enhanced efficiency in gas–solid contact and efficient handling of coarse solid particles, when compared with fluidized beds [3,8]. In the last decades, vast studies have been conducted to gain a deeper insight into the two-phase flow phenomena and the kinetic throughput of these systems, in order to advance the knowledge for troubleshooting, design, and scale-up tasks [7,9].

Despite the vast applications and studies on spouted beds, a comprehensive knowledge of the complex two-phase hydrodynamics phenomena inside the bed has not been achieved [10], which is of determinant of the kinetic throughput of spouted beds [3]. Hence, understanding the pointwise behaviors inside the bed, such as the solids trajectories and recirculation, is fundamental

for the optimization of spouted beds. In this regard, the contributions of Ali, Aradhya, Al-Juwaya, and Al-Dahhan can be highlighted [10–15]. In their work, they conducted several experimental studies on spouted beds of different sizes, with different packings and under different operation conditions, applying different advanced measurement techniques, such as g-ray CT [10,11], radioactive particle tracking (RPT) [12,13], and two-tip optical fiber probes [14,15]. In a series of contributions, they characterized the time-averaged cross-sectional solids holdup and time-averaged radial solids velocity, and developed a new scale-up technique based on radial holdup similarity.

Nevertheless, it can be recognized that despite the advances in the measurement techniques, the experimental studies are usually constrained by the applied experimental technique, leading to systematic errors [16,17], restricting the data sampling to a limited number of locations inside the bed [18], or failing to provide detailed timewise evolution of the local fields [10]. As an alternative, the mathematical modeling of spouted beds through CFD techniques has been recognized as promising tool that can provide pointwise and timewise predictions of the gas and solid behavior inside spouted beds [8,19–21]. However, in order for the models to be applicable for design, troubleshooting, and scale up tasks, there is a fundamental need for validation of the models' predictions, and to assess their predictive quality and limitations.

In the context of mathematical modeling of spouted beds, two main kinds of model can be found in literature: (i) Eulerian–Lagrangian models [17,20,22–25], also known as CFD-discrete element model (CFD-DEM) or discrete particle models (DPM), where the solid phase is modeled by solving equations of motion for each individual particle, and the multiphase interaction is included through interfacial momentum exchange sub-models; and (ii) Eulerian–Eulerian models [26–28], usually referred as Euler-2-phase (E2P) or two-fluid model (TFM), where both the solid and gas phases are treated as interpenetrating continuum, and hence, the multiphase interactions are included through effective volumetric momentum exchange sub-models. The CFD-DEM models are usually limited by the available computational resources [29], and thus, their applicability is currently constrained to small scale units. Hence, in order to model large scale units, and to enable design and scale-up tasks, the E2P models are usually preferred.

In general, regarding E2P models for gas–solid fluidized systems, two different kind of contributions can be recognized in literature, which were originally developed for fluidized beds, where the main difference is the approximation of the solids stress–strain tensor (τ_σ). The first approach, which is commonly used nowadays, is the so-called kinetic theory of granular flow (KTGF), which was first presented by Chapman and Cowling [30–32]. In this approach, an effective solid-phase stress tensor is estimated based on the concepts of the kinetic gas theory [30,33]. In order to account for the particle streaming and collisional contributions, a set of constitutive relations need to be included on the model. These relations are additional closure sub-models, which account for phenomena such as the granular viscosity, granular bulk viscosity, frictional viscosity, frictional pressure, and granular temperature [34–36]. In this sense, despite that it has been observed that the KTGF approach can provide good qualitative and quantitative predictions, it should be noted that it is required to make a proper selection of vast coupled sub-models, which should be based on the underlying assumptions for their derivation and their range of applicability. Furthermore, the sub-models are usually empirical or phenomenological closure sub-models that have been developed for fluidized bed systems, and as far as the authors concern, there are no specific developments for spouted beds.

A different approach to model the intraparticle interactions (solids stress–strain tensor) that was extensively studied between 1970 and the 2000s is the so-called bed elasticity or solids pressure models ($\nabla P_\sigma = -G(\varepsilon_\beta)\nabla\varepsilon_\beta$). The theoretical basis of these sub-models are found in early contributions by Massimilla, Donsi et al. [37,38], as well as by Mutsers and Rietema et al. [39–41]. In this approach, the solids are assumed to behave as an elastic body that can compress or expand as a mechanical structure, which is reflected on changes in the bed porosity. Therefore, the solid stress–strain tensor can be assumed to be a function of the porosity, where a modulus of elasticity ($-G(\varepsilon_\beta)$) models the proportionality of the local variations of the stress–strain tensor with respect to the local gas

holdup (ε_β). In this approach, several sub-models have been proposed in order to model the modulus elasticity [31,42–44], based on fittings of experimental data. Using this approach requires the selected sub-model to estimate the modulus of elasticity to be suitable for the modeled system. One of the main advantages of considering the bed elasticity approach is that only one closure for the modulus of elasticity is required. However, it can be noted that most of the sub-models for the estimation of this term were developed between the 1970s and 1980s, and no further investigations can be found in recent years. Also, in this approach, there are no specific sub-models specifically developed for spouted beds.

Regarding the modeling of spouted beds with an E2P formulation, the contributions of Hosseini et al. [45] can be highlighted. In their contribution, they implemented an E2P model with a KTGF approach for a pseudo 2D spouted bed, based on the experimental studies of Liu et al. [46]. They compared the predictions of the same mathematical model considering a 2D and a 3D computational domain, despite that the experimental system was a pseudo 2D system with a column thickness of 15 mm. The predictions for the model implemented on both computational domains were compared against the experimental solids flow patterns and solids velocity fields reported by Liu et al. [46]. On the experimental pseudo 2D system, a glass plane was placed as the front wall, in order to use high speed cameras and particle image velocimetry (PIV) techniques to obtain the local flow fields. The results showed that the models had a good predictive quality to reproduce the solids velocity fields, with the best agreement found when using the 3D computational domain. It was observed that the model was highly sensitive to the selected specularity coefficient, which is a closure parameter to model the wall roughness. Also, a total of 11 sub-models were coupled, and no validation of the local solids holdup fields were presented. More recently, Moliner et al. [47] also reproduced the experimental system of Liu et al. [46] with an E2P model with a KTGF approach, in order to assess the sensitivity of the models predictions when coupling different sub-models. They tested different sub-models and parameters for lift and virtual mass force, drag force, granular temperature, friction packing limit, solid pressure, radial distribution, granular viscosity, restitution coefficient, and specularity coefficient. In their results, they were able to obtain an optimized solution, with suggestions on the required sub-models that led to the best predictions. Also, in the contribution of Moliner et al., the validation of the local solids holdup field was not presented.

From these contributions, it can be seen that the models' predictive quality strongly depends on the coupled sub-models. Hence, due to the high sensitivity on the E2P on the coupled sub-models, the inclusion of a vast number of sub-models, as in the KTGF approach, increases the uncertainty of their predictions and their applicability for extrapolation capabilities, which cannot be a priori assessed. The bed elasticity approach allows, to a certain extent, to reduce the number of coupled sub-models. However, such an approach has been underexplored in recent years.

In this work, a model for a spouted bed based on the bed elasticity approach, coupling a reduced number of closure sub-models is implemented, with the objective of obtaining a model which its applicability is not tightly constrained by the sub-models included. The model with these characteristics is desirable for its application on design and scale-up tasks. The validation of the model is conducted by comparison of the pointwise solids holdup predictions against experimentally determined pointwise fields obtained by our in-house developed g-ray CT, and that have been reported on previous contributions [10,11].

2. Mathematical Modeling

2.1. Geometry and Mesh

The reproduced experimental setup corresponded to a conical spouted bed of 152 mm diameter and a total height of 1019 mm, which has been used for our previous experimental studies [10,11]. Specific cases from the reported experiments were selected for validation of the implemented mathematical model. The selected cases corresponded to spouted beds with an initial bed height of $H_{\sigma,0} = 160$ mm and $H_{\sigma,0} = 325$ mm, packed with glass beads of between 1 mm and 2 mm diameter,

and where air was used as the gas phase. Further details of the experimental setup can be seen in Figure 1, and a detailed description of the apparatus and the measurement techniques is given on the next section.

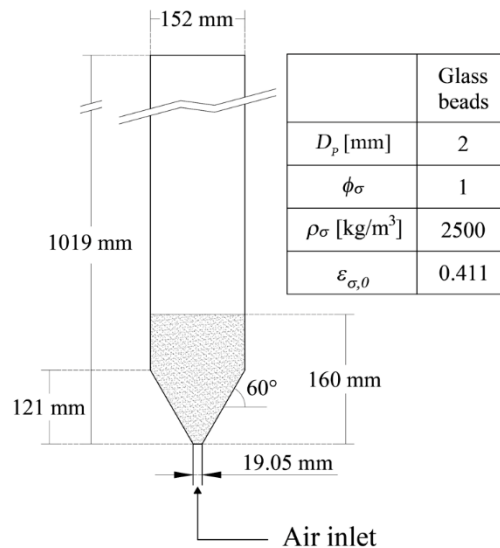


Figure 1. Details of the experimental setup for the cases with $H_{\sigma,0} = 160$ mm.

In our previous studies [10–15,48], it was observed that the solids holdup and velocity fields are axisymmetric [10,13]. Tests with different measurement techniques, under different operation conditions, and using different solid particles, have demonstrated such axisymmetric behavior [10,13]. In fact, the symmetry in the solids trajectories is one of the main advantages of spouted beds over traditional fluidized beds [3,8]. Considering this, the selected computational domain corresponded to a 2D axisymmetric domain. Details of the computational domain, the implemented mesh, and the mesh boundary layer refinement can be seen in Figure 2.

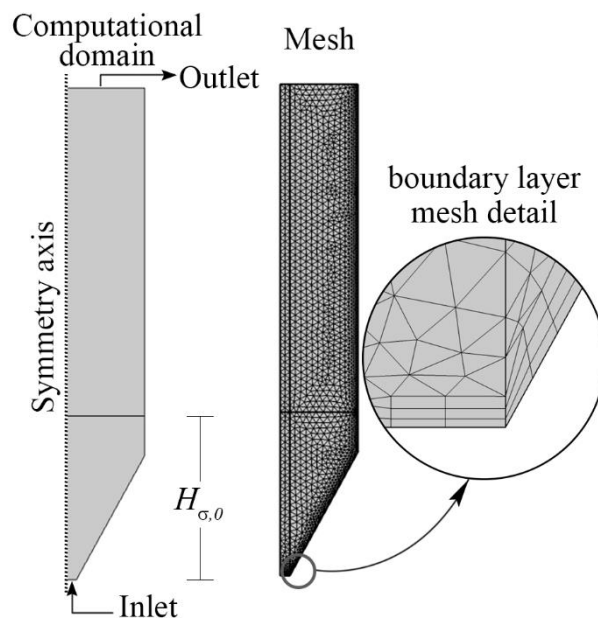


Figure 2. Computational domain and mesh details for the cases with $H_{\sigma,0} = 160$ mm.

Regarding the meshing of the computational domain, several recommendations for E2P models for gas–solid systems have been conducted and can be found in literature. In this sense, the contribution of Uddin and Coronella [49] can be highlighted, who analyzed different element mesh sizes for fluidized beds packed with particles of diameters between 212–400 μm . They determined that having a mesh element size of $18 D_p$ leads to mesh independent results. Nevertheless, when using such criteria for spouted beds, where the column to particle diameter ratio is lower, the obtained mesh could be too coarse. For the cases studied in this work, implementing Uddin and Coronella criteria leads to a mesh with an element size between 18–36 μm , which cannot provide an accurate resolution of small regions, such as the inlet. Thus, it can be seen that despite that the meshing of computational domains for E2P models for gas–solid systems has been previously studied, there is still no criteria for gas–solid systems with a low column to particle diameter ratio.

Due to this lack of criteria, in order to obtain mesh independent results, a mesh dependency analysis was conducted. Figure 3 shows a sample of the conducted mesh independency analysis, considering the time evolution of the pressure drop per unit length as a metric, for a spouted bed packed with 2 mm glass beads, with an initial bed height of $H_{\sigma,0} = 160\text{mm}$, operating at a dimensionless gas inlet velocity of $\langle V_{\beta} \rangle_0 / V_{ms} = 1.4$. The figure legend shows the relative difference from the metric predicted by a certain mesh with respect to the previous coarser mesh. In the figure, it can be seen that the change in the prediction of the pressure drop per unit length from the mesh with 10,510 cells with respect to the mesh with 5689 cells is of 8.6%. Hence, according to these results, the mesh of 5689 cells was selected. Such mesh considered triangular elements, and had a boundary layer refinement on the walls using quadrangular elements. A total of three mesh boundary layer refinements were included in the mesh. The minimum cell size considered in the mesh was 0.03 mm with a maximum growth rate to the adjacent mesh elements of 10%, and a maximum allowed cell size of 2.13 mm. The final mesh consisted of a total of 5689 elements, from which 833 corresponded to quadrangular cells on the boundary layer refinement.

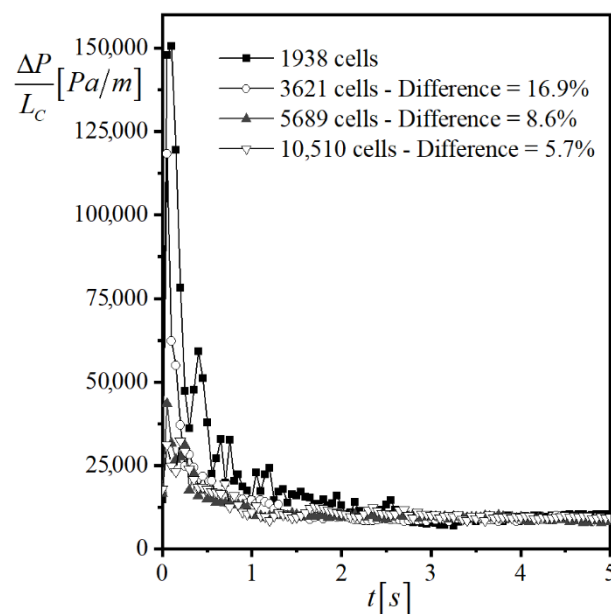


Figure 3. Sample of the mesh independency analysis, considering the pressure drop per unit length as metric, for a spouted bed packed with 2 mm glass beads, $H_{\sigma,0} = 160\text{ mm}$ and $\langle V_{\beta} \rangle_0 / V_{ms} = 1.4$.

2.2. Governing Equations

A time dependant E2P formulation with a solids pressure approach was selected to model the spouted bed. In the implemented model, the gas phase was treated as a continuous phase (β – phase) with dispersed solids (σ – phase). Both phases are treated as an interpenetrating continuum.

Equations (1) and (2) describe the continuity equation and momentum balance for the gas phase (β), respectively; while Equations (3) and (4) describe the continuity equation and momentum balance for the solid pseudophase (σ). Equation (4) in this solids pressure approach is based on the derivations of Enwald et al. [50], for which the disperse phase (σ) density is required to be several orders of magnitude larger than the continuous phase (β) density ($\rho_\sigma \gg \rho_\beta$).

$$\frac{\partial(\rho_\beta \varepsilon_\beta)}{\partial t} + \nabla \cdot (\rho_\beta \varepsilon_\beta \mathbf{v}_\beta) = 0 \quad (1)$$

$$\varepsilon_\beta \rho_\beta \left[\frac{\partial \mathbf{v}_\beta}{\partial t} + \mathbf{v}_\beta \nabla \cdot \mathbf{v}_\beta \right] = \varepsilon_\beta \left[-\nabla P + \mu_\beta (\nabla \mathbf{v}_\beta + (\nabla \mathbf{v}_\beta)^T) - \frac{2}{3} (\nabla \cdot \mathbf{v}_\beta) \mathbf{I} \right] + \rho_\beta \mathbf{g} + \mathbf{F}_d \quad (2)$$

$$\frac{\partial \varepsilon_\sigma}{\partial t} + \nabla \cdot (\varepsilon_\sigma \mathbf{v}_\sigma) = 0 \quad (3)$$

$$\varepsilon_\sigma \rho_\sigma \left[\frac{\partial \mathbf{v}_\sigma}{\partial t} + \mathbf{v}_\sigma \nabla \cdot \mathbf{v}_\sigma \right] = -\varepsilon_\sigma \nabla P - G(\varepsilon_\beta) \nabla \varepsilon_\beta + \varepsilon_\sigma \nabla \cdot [\mu_{eff} (\nabla \mathbf{v}_\sigma + (\nabla \mathbf{v}_\sigma)^T)] + \varepsilon_\sigma \rho_\sigma \mathbf{g} - \mathbf{F}_d \quad (4)$$

$-G(\varepsilon_\beta)$ and \mathbf{F}_d are the modulus of elasticity and the drag force volumetric term, respectively. ε_i is the i -phase holdup, and ρ_i is the i -phase density. μ_β and μ_{eff} are the dynamic gas viscosity and the effective solids viscosity, respectively.

On the formulation of Equation (4), in order to approximate the solids stress tensor ($\boldsymbol{\tau}_\sigma$) two contributions are considered: (i) an elastic contribution ($-G(\varepsilon_\beta) \nabla \varepsilon_\beta$), according to Equations (5) and (6) [42,51], and (ii) a viscous contribution ($\varepsilon_\sigma \nabla \cdot [\mu_{eff} (\nabla \mathbf{v}_\sigma + (\nabla \mathbf{v}_\sigma)^T)]$), modeled according to Equation (7), as suggested by Gidaspow [52]. This effective solids viscosity model provides an scale estimate of the effective solids viscosity, and satisfies that the effective solids viscosity tends to zero as the solids holdup approach to zero and provides numerical robustness.

$$\nabla \cdot \boldsymbol{\tau}_\sigma = \frac{\partial \tau_{xx}}{\partial \varepsilon_\beta} \frac{\partial \varepsilon_\beta}{\partial x} + \frac{\partial \tau_{yy}}{\partial \varepsilon_\beta} \frac{\partial \varepsilon_\beta}{\partial y} + \frac{\partial \tau_{zz}}{\partial \varepsilon_\beta} \frac{\partial \varepsilon_\beta}{\partial z} = \sum_i \frac{\partial \tau_{ii}}{\partial \varepsilon_\beta} \frac{\partial \varepsilon_\beta}{\partial i}; \sum_i \frac{\partial \varepsilon_\beta}{\partial i} = \nabla \varepsilon_\beta \quad (5)$$

$$\sum_i \frac{\partial \tau_{ii}}{\partial \varepsilon_\beta} = -G(\varepsilon_\beta) \quad (6)$$

$$\mu_{eff} = \frac{1}{2} \max(\varepsilon_\sigma, 1 \times 10^{-4}) \quad (7)$$

As far as the authors are concerned, there is no modulus of elasticity developed specifically for spouted beds. In fact, most of the experiments conducted to determine the modulus of elasticity were conducted using fine particles [39,40,42,53], while spouted beds are commonly used to handle coarse solid particles. Hence, it could expect that the currently available modulus of elasticity sub-models are not suitable for spouted beds modeling. In order to obtain a modulus of elasticity for spouted beds, the early contributions of Orr can be considered [54], which, as formulated by Bouillard et al. [43], show that a generalized form of the modulus of elasticity can be described by Equation (8).

$$G(\varepsilon_\beta)/G_0 = \exp[-c(\varepsilon_\beta - \varepsilon'_\beta)] \quad (8)$$

where c is a compaction modulus, ε'_β is the compaction gas phase volume fraction, G_0 is merely a normalizing units factor, which was considered to be 1 Pa.

Several modulus of elasticity sub-models reported on literature were tested. The parameters for such sub-models for Equation (8) can be seen in Table 1. However, all the tested sub-models led to important deviations in the prediction of the local solids holdup fields. Such deviations can be attributed to the fact that, as previously mentioned, these sub-models were developed for fluidized beds, where finer particles are used. In fact, it can be seen that in Gidaspow and Syamlal [44] and

Ettehadieh and Gidaspow [42] sub-models, the compaction gas phase volume fraction (ε'_β) is large, which corresponds to fine particles. Hence, in order to overcome the limitations of the available sub-models, a new modulus of elasticity is proposed on this work, based on a sensitivity study to fit the parameters of Equation (8), in order to obtain the parameters which led to the most accurate predictions of the experimental data. Such a sensitivity study was conducted by running a parametric sweep of the compaction modulus and compaction gas phase volume fraction. Considering that ε'_β physically represent the volume fraction of gas flowing through the bed without expansion (i.e., the minimum allowed gas holdup), the parametric sweep considered values of ε'_β between 0.35–0.45 with increments of 0.01, leading to 11 tested values. For the compaction modulus, there is no clear physical meaning, and thus, based on other experimental works, such as the work of Bouillard et al. [43] and the work of Gidaspow and Syamlal [44], large c values were tested, rather than small values, as in the case of the sub-model proposed by Ettehadieh and Gidaspow [42]. The values of c in the parametric sweep ranged between 500–1000 considering increments of 50, leading to 11 tested values. In this way, a total of 121 cases were set, and the predictions were compared against experimental results. It should be pointed out that several of the cases did not converge, all of the cases with a c value equal or greater to 850 did not converge. The case with $c = 750$ and $\varepsilon'_\beta = 0.38$ led to the closest predictions. It can be seen that the optimum value of ε'_β corresponds to a maximum packing of 0.62, which is a typical value found in beds packed with spherical particles [55].

Table 1. Modulus of elasticity sub-model parameters.

c	ε'_β	Reference
600	0.376	Bouillard et al. [43]
500	0.422	Gidaspow and Syamlal [44]
20	0.62	Ettehadieh and Gidaspow [42]
750	0.38	This work

Figure 4 shows a comparison of the predicted modulus of elasticity by the different sub-models tested against the gas holdup. It can be seen that the sub-model proposed on this work, based on the sensitivity analysis, resembles more the sub-model proposed by Bouillard et al. [43] than the other two sub-models tested. The main difference between the sub-model proposed by Bouillard et al. [43] and the sub-model proposed in this work is in the compaction modulus (c). It can be noted that the natural logarithm of the modulus of elasticity ($\ln\left[\frac{G(\varepsilon_\beta)}{G_0}\right]$) of the proposed sub-model has a steeper slope, and becomes zero faster than Ettehadieh and Gidaspow [42] and Gidaspow and Syamlal [44] sub-models. As it will be shown in the results, these differences lead to enhanced predictions of the pointwise gas holdup when compared with the most common modulus of elasticity sub-model, such as Ettehadieh and Gidaspow [42] and Gidaspow and Syamlal [44] sub-models. However, it should be kept in mind that the proposed model is based on a sensitivity study, and hence, there is no mechanistic development of this new model. Further research efforts in the development of a mechanistic modulus of the elasticity sub-model are still desirable.

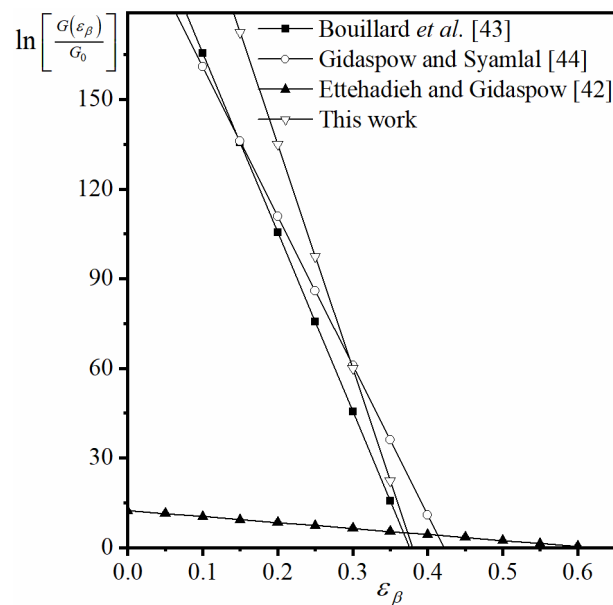


Figure 4. Comparison of the predicted modulus of elasticity of the different sub-models tested.

The second sub-model included is a volumetric momentum exchange term, the drag force (F_d), which accounts for the multiphase interactions. As noted on Equations (2) and (4), the implemented drag force model assumes that the force acting on both phases has the same magnitude, but is working on opposite directions. The drag force is modeled according to Equation (9), where $K_{\sigma\beta}$ is the multiphase interaction coefficient. This multiphase interaction coefficient is modeled according to Equation (9) [56], where C_D is the drag coefficient.

$$\mathbf{F}_d = K_{\sigma\beta}(\mathbf{v}_\sigma - \mathbf{v}_\beta) = K_{\sigma\beta}\mathbf{v}_{slip} \quad (9)$$

$$K_{\sigma\beta} = \frac{3}{4D_P}\varepsilon_\sigma C_D \rho_\beta |\mathbf{v}_{slip}| \quad (10)$$

In literature related to the modeling of spouted beds, it can be seen that there is not an universally accepted drag force or drag coefficient sub-model, even though, most of the recent works implement the Gidaspow [52] or Syamlal-O'Brien [57] models. In fact, it might seem that the selection of these two drag force sub-models is motivated by common practices on modeling fluidized beds. However, the gas–solid interactions in spouted beds, where coarse particles are involved, cannot be assumed to be the same as the interactions in fluidized beds. Several works have been conducted in order to determine the drag force sub-model for spouted beds which lead to the most accurate predictions of experimental measurements [21,36,47]. In such works, it has been recognized that the models' predictive quality is highly sensitive to closure parameters of the implemented sub-model, which are usually empirical closure parameters for empirical sub-models. Thus, a proper identification of the adequate parameters is mandatory to obtain a predictive model. This represents a major issue for the application of the implemented models for extrapolation studies, as there is no way to assess whether the identified parameters are adequate for a different system or different operation conditions. Hence, there is still a need to develop new drag force models which are suitable for spouted beds, which do not depend on the inclusion of a vast number of empirical closure parameters, and which have a mechanistic or phenomenological development in order to enhance their applicability for extrapolation studies.

In this work, the drag coefficient on Equation (10) is modeled according to the sub-model proposed by Ishii and Zuber [58], as described by Equation (11). Such model was developed as a generalization of the sub-model proposed by Schiller and Naumann [59]. The sub-model proposed by Schiller and

Naumann has a mechanistic foundation, based on the flow around a single sphere, and provides a close approximation of the standard drag curve for a non-rotating sphere [56]. Based on the work of Schiller-Naumann, Ishii, and Zuber [58] proposed a generalization for a drag coefficient in bubbly, droplet or particulate flows, leading to a phenomenological drag force sub-model. They introduced the mixture viscosity concept to the drag coefficient formulations to develop a generalized model that could be adapted for gas–liquid flows as well as for gas–solid flows.

$$C_D = \max \left[\frac{24}{\text{Re}_{mix}} (1 + 0.1 \text{Re}_{mix}^{0.75}), 0.45 \left(\frac{1 + 17.67 \left(\frac{\varepsilon_\beta^{0.5} \mu_\beta}{\mu_{mix}} \right)^{6/7}}{18.67 \frac{\varepsilon_\beta^{0.5} \mu_\beta}{\mu_{mix}}} \right) \right] \quad (11)$$

$$\text{Re}_{mix} = \frac{D_P \rho_\beta |\mathbf{v}_{slip}|}{\mu_{mix}} \quad (12)$$

$$\mu_{mix} = \mu_\beta \left(1 - \frac{\varepsilon_\sigma}{\varepsilon_\sigma^{\max}} \right)^{-2.5 \varepsilon_\sigma^{\max}} \quad (13)$$

where Re_{mix} is the mixture effective Reynolds number, described by Equation (11). μ_{mix} is a mixture effective viscosity, modeled according to a Krieger type sub-model [55] described by Equation (12). Where $\varepsilon_\sigma^{\max}$ is the maximum solids packing, which was set as $\varepsilon_\sigma^{\max} = 1 - \varepsilon'_\beta$.

The following boundary conditions are set to the described model.

$$-\mathbf{n} \cdot \mathbf{v}_\beta = f(t) \langle V_\beta \rangle_0 \quad (\text{inlet}) \quad (14)$$

$$\mathbf{v}_\sigma = 0 \quad (\text{inlet}) \quad (15)$$

$$\varepsilon_\sigma \mathbf{v}_\sigma \cdot \mathbf{n} = 0 \quad (\text{inlet}) \quad (16)$$

$$\varepsilon_\beta \left[\mu_\beta (\nabla \mathbf{v}_\beta + (\nabla \mathbf{v}_\beta)^T - \frac{2}{3} (\nabla \cdot \mathbf{v}_\beta) \mathbf{I}) \right] \mathbf{n} = 0 \quad (\text{outlet}) \quad (17)$$

$$\left\{ -G(\varepsilon_\beta) \nabla \varepsilon_\beta + \varepsilon_\sigma \nabla \cdot [\mu_{eff} (\nabla \mathbf{v}_\sigma + (\nabla \mathbf{v}_\sigma)^T)] \right\} \mathbf{n} = 0 \quad (\text{outlet}) \quad (18)$$

$$P = P_0 \quad (\text{outlet}) \quad (19)$$

$$\mathbf{v}_\beta = 0 \quad (\text{walls}) \quad (20)$$

$$\mathbf{v}_\sigma \cdot \mathbf{n} = 0 \quad (\text{walls}) \quad (21)$$

$$\varepsilon_\sigma \mathbf{v}_\sigma \cdot \mathbf{n} = 0 \quad (\text{walls}) \quad (22)$$

$$\mathbf{v}_\beta \cdot \mathbf{n} = 0 \quad (\text{symmetry axis}) \quad (23)$$

$$\mu_\beta (\nabla \mathbf{v}_\beta + (\nabla \mathbf{v}_\beta)^T - \frac{2}{3} (\nabla \cdot \mathbf{v}_\beta) \mathbf{I}) \mathbf{n} \quad (\text{symmetry axis}) \quad (24)$$

$$-\mu_\beta (\nabla \mathbf{v}_\beta + (\nabla \mathbf{v}_\beta)^T - \frac{2}{3} (\nabla \cdot \mathbf{v}_\beta) \mathbf{I}) \mathbf{n} \cdot \mathbf{n} = \mathbf{n} \quad (\text{symmetry axis}) \quad (25)$$

$$\mathbf{v}_\sigma \cdot \mathbf{n} = 0 \quad (\text{symmetry axis}) \quad (25)$$

$$\left\{ \frac{-G(\varepsilon_\beta) \nabla \varepsilon_\beta}{\varepsilon_\sigma} + \nabla \cdot [\mu_{eff} (\nabla \mathbf{v}_\sigma + (\nabla \mathbf{v}_\sigma)^T)] \right\} \mathbf{n} \quad (\text{symmetry axis}) \quad (26)$$

$$-\left\{ \frac{-G(\varepsilon_\beta) \nabla \varepsilon_\beta}{\varepsilon_\sigma} + \nabla \cdot [\mu_{eff} (\nabla \mathbf{v}_\sigma + (\nabla \mathbf{v}_\sigma)^T)] \right\} \mathbf{n} \cdot \mathbf{n} = \mathbf{n}$$

where \mathbf{n} is the normal vector to the surface of the prescribed boundary. Equations (14)–(16) prescribe that the inlet is pure air. Equation (14) includes a function of time ($f(t)$) multiplied by the superficial inlet velocity, which allows to reproduce the start-up of the spouted bed. $f(t)$ is a smoothstep function, which starts in a value of zero and smoothly increases to a value of 1, in a transition zone of 0.002 s. Such transition follows a sigmoid curve shape, and after the transition zone, the value of the function is held constant with a value of 1. In this way, the effect of the increase in the inlet velocity in the start-up of the experimental apparatus is, to a certain extent, captured. Furthermore, the inclusion of this time function enhances the numerical stability of the model during the initial physical times simulated. Equations (17)–(19) indicate that the outlet pressure is atmospheric, and that there is no viscous stress for the gas and solid phases on the outlet boundary. Equation (20) establishes a no-slip boundary condition for the gas phase, while Equations (21) and (22) set a free-slip boundary condition for the solid phase. Finally, Equations (23)–(26) describe the axial symmetry. Equations (23) and (25) prescribe that the radial velocity component for both phases is zero at the

symmetry axis; while Equations (24) and (26) establish that the stress of each phase vanishes in the z direction, as it approaches the symmetry axis.

2.3. Computation

The model mathematical model described on the previous sub-sections was implemented on the commercial software Comsol Multiphysics 5.5, which uses a Finite Element Method approach. The simulations were run on a workstation equipped with a single socket Intel® Xeon® W-2175 processor, which has 14 physical cores and 28 threads, and runs at a base frequency of 2.5 GHz. The simulations were run using all the cores, allowing an overclocking on the cores' frequency to a maximum of 4.3 GHz. The workstation was equipped with 256 Gb of RAM, but the simulations only required a maximum of 4 Gb of RAM. With these specifications, the simulation cases, considering physical times of up to 10 s, took solution times of around 1 h. However, as it will be discussed in the following section, a physical time of 5 s was enough to capture the steady state behavior of the simulated spouted bed cases, and thus, the solution times were reduced to under 40 min.

The unsteady problem was computed implementing an implicit time-stepping method using a backward differentiation formula (BFD). For numerical stability, the initial time step was set to be 1×10^{-5} s and the maximum allowed time step was constrained to be 0.001 s. The time steps taken by the solver were allowed to be freely selected by the internal algorithm of the software. The solution was stored every 0.05 s increments in the physical time.

In order to handle the non-linear steady problem, a segregated solver sequence was implemented. In this solver sequence, the variables were separated in two different sub-groups, one for the gas volume fraction (ε_β), and one for the hydrodynamic variables ($P, \mathbf{v}_\sigma, \mathbf{v}_\beta$). Uzawa iterations are considered to compute each step for the sub-groups. This is, one sub-group is held constant while the other one is being computed. To compute each sub-group, a direct linear solver was selected, using a parallel sparse direct solver (PARDISO), which is incorporated in Comsol Multiphysics.

3. Experimental Work

3.1. Apparatus and Operation Conditions

Vast experimental studies on spouted beds have been conducted by our research group and has been reported on a series of contributions from recent years [10–15,48]. The apparatus used on these experimental studies corresponds to the one shown in Figure 1, and another scaled-down unit based on the setup shown in Figure 1. In order to assess the effect of the solid particles' properties, different particles were used, such as glass beads and steel shots of different diameters. Accordingly, several operation conditions, such as different inlet gas flow rate and static bed height, were tested and reported on these previous contributions.

From this extensive data base of experiments, selected experiments were chosen as benchmarking experiments to be reproduced by the mathematical model, in order to assess the predictive quality and limitations of the described model. The selected cases correspond to spouted beds packed with glass beads between 1 mm and 2 mm diameter, with static bed heights of 160 mm and 325 mm. Further details of the geometrical characteristics and experimental conditions are summarized in Table 2.

Table 2. Geometrical properties of the experimental setup and operation conditions.

Geometry			
D_C [mm]	15.2		
L_C [mm]	1019		
D_i [mm]	19.05		
H_{cone} [mm]	121		
γ_{cone} [°]	60		
Solids(σ - phase)			
Case	I	II	III
Material	Glass beads	Glass beads	Glass beads
$H_{\sigma,0}$ [mm]	160	160	325
D_P [mm]	1	2	1.41
ρ_σ [kg/m ³]	2500	2500	2500

Experiments were conducted at different dimensionless gas inlet velocities ($\langle V_\beta \rangle_0 / V_{ms}$), between $\langle V_\beta \rangle_0 / V_{ms} = 1.1 - 1.4$. The minimum spouting velocity (V_{ms}) was estimated according to the approach and correlations proposed by San José et al. [60]. According to San José et al. [60], the minimum spouting velocity on cylindrical spouted beds has two contributions, one dependant on the cone section, and one on the cylinder section, as described by Equation (27). The cone and cylinder contributions are estimated according to the correlations shown in Equations (28) and (29), respectively.

$$V_{ms} = (V_{ms})_{cone} + (V_{ms})_{cylinder} \quad (27)$$

$$(V_{ms})_{cone} = \left(\frac{D_i^2}{D_C^2} \right) \left(\frac{\mu_\beta}{\rho_\beta D_P} \right) (\text{Re}_0)_{ms}^{cone}; \quad (\text{Re}_0)_{ms}^{cone} = 0.126 \text{Ar}^{0.5} \left(\frac{D_C}{D_i} \right)^{1.68} \left[\tan \left(\frac{\gamma_{cone}}{2} \right) \right]^{-0.57} \quad (28)$$

$$(V_{ms})_{cylinder} = \left(\frac{D_P}{D_C} \right) \left(\frac{D_i}{D_C} \right)^{0.1} \left[2g(H_{\sigma,0} - H_{cone}) \left(\frac{\rho_\sigma - \rho_\beta}{\rho_\beta} \right) \right]^{0.5} \quad (29)$$

3.2. γ -ray Computed Tomography (CT)

The experimental studies on the selected cases were conducted applying our in-house developed advanced γ -ray computed tomography (CT) [10,61]. This is a non-invasive radioisotopes-based technique, which allows to obtain the time averaged cross-sectional phases holdup distribution. The technique consists of a collimated γ -ray source that provides a 40° γ -ray fan beam, which faces an arch array of 15 sodium iodide (NaI (T1)) scintillation detectors. The source is Cs-137 (193 mCi, 661 keV, 30.07 years half-life), which is housed in a lead container. Both the source and the detectors are placed on a platform that can fully rotate around the column, and that can move up and down.

Considering the rotation of the platform, at each selected axial position, a series of 197 views are obtained in each scan, which correspond to 197 different source positions. At each position, the detector arch array moves to 21 different positions. Each of these scans, moving through all the positions, is finished in around 6 h. The raw data obtained by the CT scans is then processed by using an alternating minimization algorithm [61].

In this way, the CT technique allows to obtain time averaged cross-sectional phases holdup distribution along the column height.

4. Results and Discussion

The results from the mathematical model allowed to obtain pointwise and timewise solids and liquid hydrodynamic variables fields, such as pressure, superficial velocity, and holdup. In order to compare such results with the CT scans results, a time average was considered in the predicted solids holdup fields. The time averaged discarded the initial two seconds of the simulation to avoid

the start-up effects. Thus, the time averaged field of any variable (ψ) was estimated according to Equation (30).

$$\langle \psi \rangle_t = \frac{1}{t_{total} - 2s} \int_{2s}^{t_{total}} \psi dt \quad (30)$$

where t_{total} is the total time simulated, which varied depending on the case. For the shallow spouted beds ($H_{\sigma,0} = 160$ mm) the steady operation was obtained after one second, and hence, a physical time of 5 s was enough to obtain a representative time average. However, for the cases with $H_{\sigma,0} = 325$ mm a physical time of 10 s was required, as the steady state took longer to be reached, in around 2 s. Figure 5 shows the timewise series of the absolute pressure and solids holdup evaluated in the center line of the computational domain ($r = 0$) at different axial locations (z), for the case of a spouted bed packed with 2 mm diameter glass beads, $H_{\sigma,0} = 160$ mm, operating at $\langle V_{\beta} \rangle_0 / V_{ms} = 1.2$. It can be seen that both the solids holdup and absolute pressure timewise changes reach a stable value after one second. The evaluated coefficient of variation ($CoV = SD_{\psi,t} / \langle \psi \rangle_t$) considering $t > 1$ s is also shown in the figure. Increasing the physical time simulated did not show a change in the stable value reached, nor a significant change in the evaluated CoV . Hence, these results suggest that a simulated physical time of 5 s, is enough to capture the steady state behavior of a spouted bed packed with 2 mm diameter glass beads, $H_{\sigma,0} = 160$ mm, operating at $\langle V_{\beta} \rangle_0 / V_{ms} = 1.1$. Similar analyses were made for the different cases in order to determine the adequate physical time to obtain representative predictions of the steady state behavior.

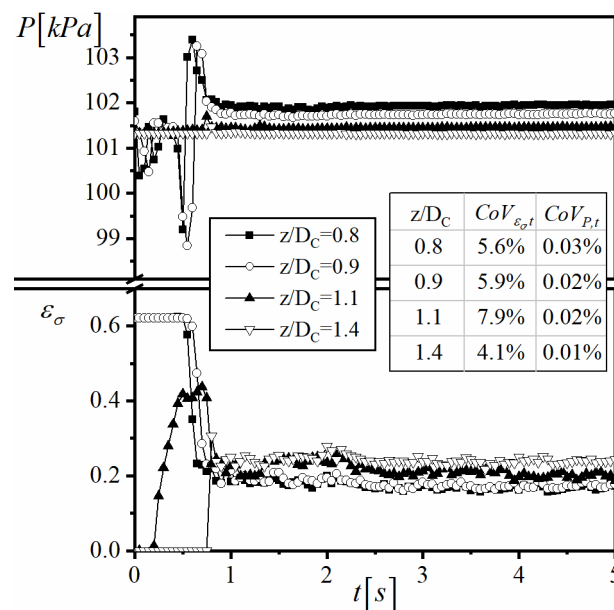


Figure 5. Timewise change of the absolute pressure and solids holdup at different axial locations and $r = 0$ in a spouted bed packed with 2 mm glass beads, $H_{\sigma,0} = 160$ mm and $\langle V_{\beta} \rangle_0 / V_{ms} = 1.2$.

4.1. Influence of the Modulus of Elasticity Sub-Model

Simulations were run using the different modulus of elasticity sub-models listed in Table 1 and compared in Figure 3. A comparison of the time averaged predicted radial solids holdup by the model using the different modulus of elasticity sub-models is shown in Figure 6a–c. As expected from the comparison in Figure 3, the prediction obtained when implementing the sub-model proposed by Bouillard et al. [43] resembles the prediction obtained when implementing the sub-model proposed in this work. In fact, Figure 6a–c shows that the difference in the predictions between Bouillard et al. [43] case and the case with the proposed model is marginal.

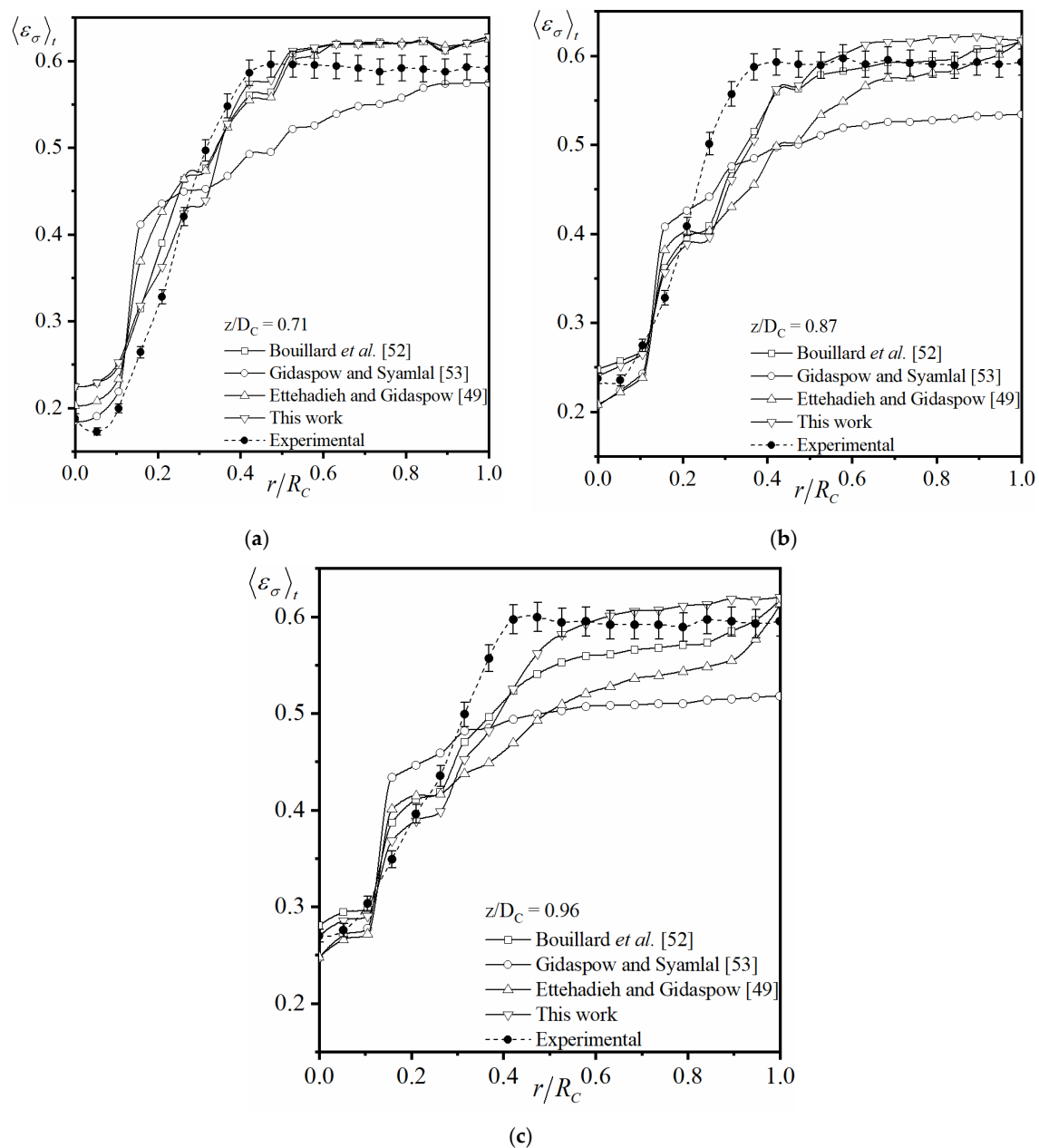


Figure 6. (a) Time-averaged predicted radial solids holdup profiles for spouted bed packed with 1 mm glass beads, $H_{\sigma,0} = 160$ mm and $\langle V_{\beta} \rangle_0 / V_{ms} = 1.1$ at (a) $z/D_C = 0.71$, (b) $z/D_C = 0.87$, (c) $z/D_C = 0.96$.

Tables 3 and 4 show the obtained average absolute relative error $\left(AARE = \frac{1}{n_i} \sum_i \left| \frac{(\psi_{CFD})_i - (\psi_{EXP})_i}{(\psi_{EXP})_i} \right| \right)$ and the mean squared deviation $\left(MSD = \frac{1}{n_i} \sum_i [(\psi_{CFD})_i - (\psi_{EXP})_i]^2 \right)$ when comparing the model prediction against experimental data, respectively. It can be seen that the obtained AARE is between 4.6–8.9% and 5.1–9.4% for the case with the proposed sub-model and the case with Bouillard et al. [43] sub-model, respectively. Also, it can be seen that the other tested models exhibit larger deviations in term of their AARE and MSD.

Table 3. Average absolute relative error (%) in the time-averaged predicted radial solids holdup profiles for spouted bed packed with 1 mm glass beads, $H_{\sigma,0} = 160$ mm and $\langle V_{\beta} \rangle_0 / V_{ms} = 1.1$.

Sub-Model				
z/D_C	Bouillard et al. [43]	Gidaspow and Syamlal [44]	Ettehadieh and Gidaspow [42]	This work
0.71	9.39	11.94	9.44	8.89
0.87	5.11	12.25	9.05	6.14
0.96	5.48	12.53	10.05	4.62
$\langle AARE \rangle$	6.66	12.24	9.51	6.55
$\langle AARE \rangle = \frac{1}{n_j} \sum_j (AARE_j)$				

Table 4. Mean squared deviation (%) in the time-averaged predicted radial solids holdup profiles for spouted bed packed with 1 mm glass beads, $H_{\sigma,0} = 160$ mm and $\langle V_{\beta} \rangle_0 / V_{ms} = 1.1$.

Sub-Model				
z/D_C	Bouillard et al. [43]	Gidaspow and Syamlal [44]	Ettehadieh and Gidaspow [42]	This work
0.71	0.13	0.41	0.18	0.12
0.87	0.13	0.46	0.36	0.18
0.96	0.11	0.53	0.39	0.10
$\langle MSD \rangle$	0.12	0.46	0.31	0.13
$\langle MSD \rangle = \frac{1}{n_j} \sum_j (MSD_j)$				

These results suggest that the model predictions are sensible to the implemented sub-model, and that an improvement in the modulus of elasticity sub-model is required to enhance the predictive quality of the model. As previously stated, currently there is no modulus of elasticity sub-model developed for spouted beds, and hence, further research in developing a modulus of elasticity sub-model for spouted beds based on a mechanistic development is yet desirable. One of the main reasons for this lack of a modulus of elasticity for spouted beds is that the current trend when modeling spouted beds is the implementation of a KTGF approach [8,21,45,47]. However, the KTGF approach relies on the inclusion of a vast number of sub-models, which are usually empirical or semi-empirical sub-models, which could over-constrain the range of applicability of the models, hence, constraining their extrapolation capabilities.

These results suggest that the model predictions are sensible to the implemented sub-model, and that an improvement in the modulus of elasticity sub-model is required to enhance the predictive quality of the model. As previously stated, currently there are no modulus of elasticity sub-model developed for spouted beds, and hence, further research in developing a modulus of elasticity sub-model for spouted beds based on a mechanistic development is yet desirable. One of the main reasons for this lack of a modulus of elasticity for spouted beds is that the current trend when modeling spouted beds is the implementation of a KTGF approach [8,26,27,54]. However, the KTGF approach relies on the inclusion of a vast number of sub-models, which are usually empirical or semi-empirical sub-models, which could over-constrain the range of applicability of the models, thus constraining their extrapolation capabilities.

4.2. Comparison with Experiments

Figure 7 shows a comparison between the obtained cross-sectional time-averaged solids holdup from the CT scans and the model predictions. It can be noted that there is a good qualitative similarity between the experimental results and the model predictions. From the experimental observations,

the spout diameter can be appreciated to be in close agreement with the experimental observation. The implemented model considered a 2D axisymmetric domain; however, for comparison purposes, the results shown in Figure 7 correspond to the projection of the axisymmetric solution. Thus, the model predictions shown in the figure are perfectly symmetric. When compared with the experimental result, it can be seen that the symmetric behavior is also observed on the CT scans. Such symmetric behavior on spouted beds has already been reported [3,8], and was demonstrated on our previous contributions [10,13]. Hence, the results obtained by the CT scans, and the comparison shown in Figure 7 support the assumption that a 2D axisymmetric computational domain is representative enough to capture the pointwise solids distribution on a spouted bed.

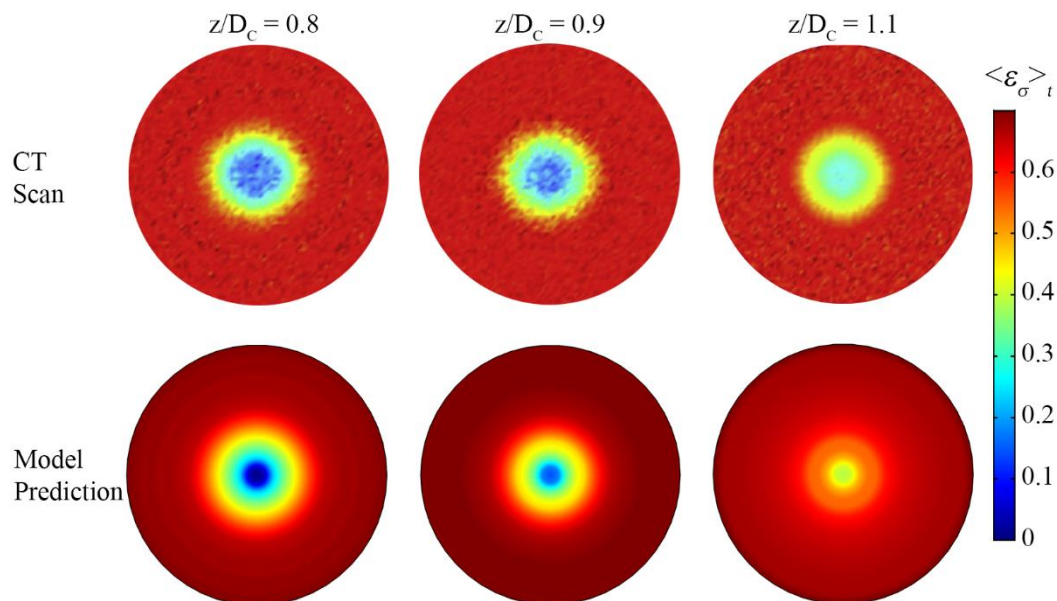


Figure 7. Comparison between CT scan results and model prediction of the time averaged cross-sectional solids holdup distribution for a spouted bed packed with 2 mm glass beads, $H_{\sigma,0} = 160$ mm and $\langle V_{\beta} \rangle_0 / V_{ms} = 1.1$.

Considering that the experimental cross-sectional time-averaged solid holdup distributions are symmetric, it is possible to estimate an azimuthal average of the fields, in order to obtain a local comparison with the model predictions. The azimuthal average is estimated according to Equation (31).

$$\langle \psi \rangle_{\theta,t} = \frac{1}{2\pi} \int_0^{2\pi} \langle \psi \rangle_t d\theta \quad (31)$$

Considering the time and azimuthal average of the experimentally measured fields, Figure 8a–d show a comparison between the model predictions and the experimental fields for a spouted bed packed with 2 mm glass beads, $H_{\sigma,0} = 160$ mm and $\langle V_{\beta} \rangle_0 / V_{ms} = 1.1$ at different axial positions. It can be appreciated that at the low axial positions ($z/D_C = 0.8, 0.9, 1.1$), there is a close agreement in the model predictions and the experimental measurements. The AARE in these cases is between 5.75% and 6.38%, and the MSD between 0.13% and 0.22%, which show that the implemented model has a good predictive quality. It should be pointed that these predictions correspond to a model considering the modulus of elasticity proposed in this work.

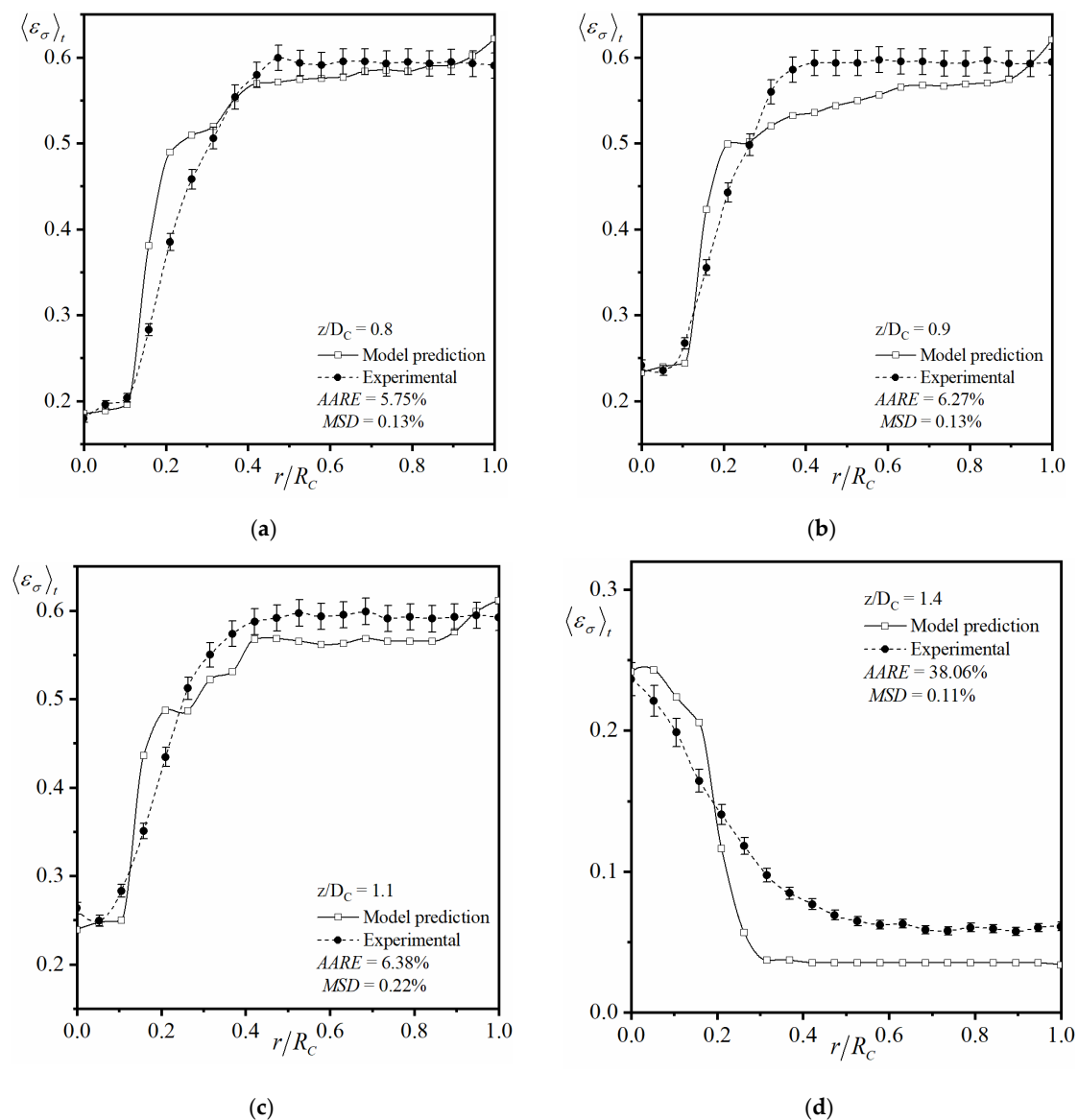


Figure 8. Experimental and model predicted time-averaged radial solids holdup distribution for a spouted bed packed with 2 mm glass beads, $H_{\sigma,0} = 160$ mm and $\langle V_{\beta} \rangle_0 / V_{ms} = 1.1$ at (a) $z/D_C = 0.8$. (b) $z/D_C = 0.9$ (c) $z/D_C = 1.1$ (d) $z/D_C = 1.4$.

From Figure 8a–d it can also be appreciated that, as the axial position increases, the deviation in the predictions increase. In this sense, it can be seen that the AARE of the prediction shown in Figure 8d, which corresponds to the axial position $z/D_C = 1.4$, is high, with a value of 38.06%. However, the MSD obtained for the same measurements is of only 0.11%. These deviation measurements show that the model fails to properly capture the values of solids holdup profile but has a good predictive quality of the trend. Such axial position corresponds to the fountain region, where the solids flow disengages, and the solid particles fall into the annulus region for recirculation. Thus, according to the comparison with the experimental profile shown in Figure 8d, it can be interpreted that the model shows a deviation in the prediction of the width of the fountain.

For the sake of comparison, Figure 9 shows the CT scan results and the projected 2D cross-sectional time averaged solids holdup distribution for the same case shown in Figure 8d. From Figure 9, the experimental measurements suggest that the fountain width is practically as wide as the column diameter. Thus, the time-averaged profiles show that the lowest solids holdup values are around 0.06. On the model predictions, it appears that the solids recirculation occurs in a narrower region, and thus,

the quantity of solids that fall through radial positions closer to the column wall is lower. In the model predictions, the lowest holdup values obtained are around 0.03. These differences between the model prediction and the experimental measurements in the fountain region can be attributed to two different factors. The first one is, as also previously discussed, the implemented sub-models. The results shown in the previous sub-section show that the model predictions are sensitive to the implemented modulus of elasticity sub-model, and hence, an improved modulus of elasticity sub-model could enhance the prediction of the solids holdup distribution on the fountain region. Further research efforts are still required in this regard. The second source of deviations could be attributed to the sensitivity and resolution of the CT technique. Despite that, the developed CT technique has been proven to provide accurate results [10,61–63], it has also been recognized in literature that, despite the implementation of advanced measurement techniques, there are still systematic errors depending on the applied technique [16,17].

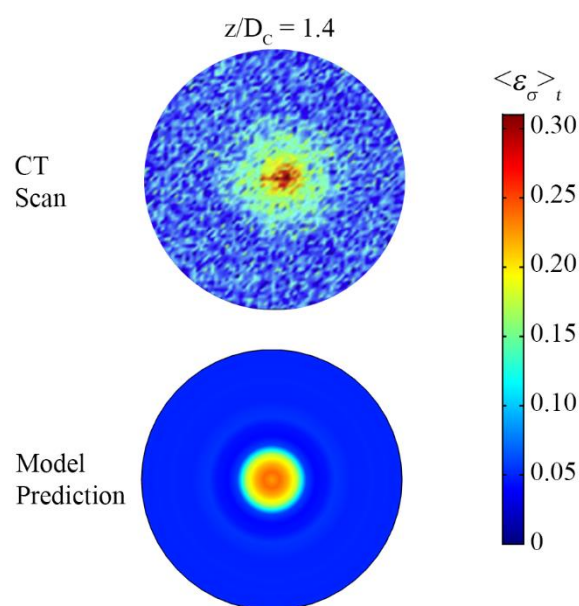


Figure 9. Comparison between CT scan results and model prediction of the time averaged cross-sectional solids holdup distribution for spouted bed packed with 2 mm glass beads, $H_{\sigma,0} = 160$ mm and $\langle V_{\beta} \rangle_0 / V_{ms} = 1.1$ at $z/D_C = 1.4$.

Similarly to Figure 8a–d, Figure 10a,b show a comparison between the azimuthally averaged experimentally measured radial solids holdup profile and the model prediction for a spouted bed packed with 1.41 mm glass beads, $H_{\sigma,0} = 325$ mm and $\langle V_{\beta} \rangle_0 / V_{ms} = 1.2$. In these figures, it can be appreciated that when changing the static bed height, solids diameter and the inlet velocity, the model still exhibits a good predictive quality. For this case, the AARE is found to be 7.26% and 6.26% when comparing with the experimental measurements at $z/D_C = 1.1$ and $z/D_C = 1.8$, respectively. The MSD is also found to be low, with values of 0.24% and 0.16% at $z/D_C = 1.1$ and $z/D_C = 1.8$, respectively.

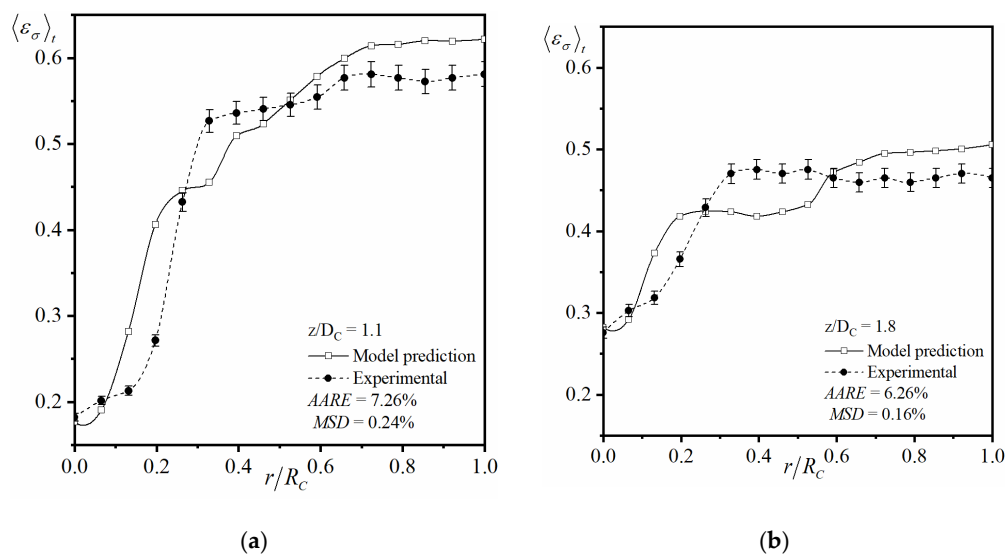


Figure 10. Experimental and model predicted time-averaged radial solids holdup distribution for a spouted bed packed with 1.41 mm glass beads, $H_{\sigma,0} = 325$ mm and $\langle V_\beta \rangle_0 / V_{ms} = 1.2$ at (a) $z/D_C = 1.1$. (b) $z/D_C = 1.8$.

Considering all the tested cases, Figure 11 shows a parity plot of the pointwise measurements and model predicted solids holdups. In this figure, it can be seen that most of the solid holdup predictions have deviations under 15%. In fact, the largest deviations are found at the lowest experimentally determined local solids holdups, which correspond to the solids holdups in the fountain regions, as previously discussed. This represents a limitation in the implemented model which, however, can be improved if an enhanced modulus of elasticity sub-model is developed for specific application on spouted beds. Nevertheless, it is important to recognize that the implemented model allows to properly predict the pointwise solids holdup profiles in the annulus and spout region for spouted beds packed with particles of different sizes, different static bed heights, and at different superficial inlet velocities.

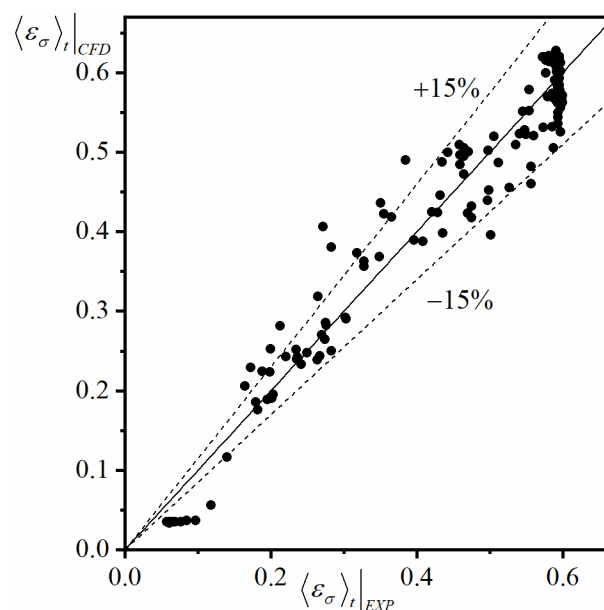


Figure 11. Parity plot of the experimentally measured and predicted pointwise solids holdup for all tested cases.

5. Remarks

A Euler–Euler model based on a solids pressure approach was implemented for predicting the local solids holdup distribution on a spouted bed. The model included a reduced number of sub-models as closures in order to enhance the applicability of the model. The model predictions were compared with experimentally measured cross-sectional solids holdup profiles obtained by application of our in-house developed γ -ray computed tomography measurement technique.

In order to enhance the model's predictive quality, a new modulus of elasticity sub-model was proposed and compared against other common sub-models reported in literature. The model predictions exhibited that the model results are sensitive to changes in the implemented modulus of elasticity. Modifications in the modulus of elasticity sub-model can improve the model predictions, and thus, there is a need to develop an enhanced modulus of elasticity sub-model which can further enhance the model predictions. The proposed model in this work allows to enhance the predictions in comparison with the results obtained by the other models found in literature. Furthermore, the implemented E2P model with the bed elasticity approach allows to reduce the number of required closure sub-model, producing a model with a lower degree of non-linearity. This allows the model to use reduced computational resources in comparison with the E2P models with a KTGF approach. The reduction of the required closure sub-models and computational resources is a desirable characteristic to model larger scale systems and enable scale-up studies. However, the sub-model proposed in this work is based on a sensitivity analysis and lacks a mechanistic development. Further research is hence needed in this regard.

Despite such limitation in the implemented modulus of elasticity sub-model, the model shows a high predictive quality when predicting the pointwise solids holdup profiles in the spout and annulus regions in spouted beds. It was observed that under different operation conditions, such as packings of different diameters, different static bed height and different inlet velocities, the model exhibits a constantly high predictive quality. Nevertheless, the model predictions show considerable deviations in the prediction of the fountain region behavior. Such deviations in the fountain region could be improved with the implementation of an enhanced modulus of elasticity sub-model. Also, to a certain extent, the sensitivity and resolution of the CT technique could also be a source of the observed deviations.

Author Contributions: Conceptualization, S.U. and M.A.-D.; methodology, investigation and formal analysis, S.U., B.Q., O.F.; writing—original draft, S.U.; writing—review and editing and project administration, M.A.-D. All authors have read and agreed to the published version of the manuscript.

Funding: This research did not receive any specific grant from funding agencies in the public, commercial, or not-for-profit sectors.

Conflicts of Interest: The authors declare no conflict of interest

Nomenclature

<i>AARE</i>	Average Absolute Relative Error	<i>Greek symbols</i>	
<i>CT</i>	γ -ray Computed Tomography	β	Gas phase
<i>C</i>	Compaction modulus	ε_i	Volume fraction (holdup) of phase <i>i</i>
<i>CFD</i>	Computational Fluid Dynamics	ε'_β	Compaction gas holdup
<i>CoV</i>	Coefficient of Variation	$\varepsilon_\sigma^{\max}$	Maximum solids packing
<i>C_D</i>	Drag coefficient	γ_{cone}	Cone angle (°)
<i>D_C</i>	Column diameter (m)	μ_i	Dynamic viscosity of phase <i>i</i> (Pa s)
<i>D_P</i>	Solid particle diameter (m)	ρ_i	Density of phase <i>i</i> (kg/m ³)
<i>E2P</i>	Euler-two-phase	θ	Angular direction
<i>F_d</i>	Volumetric drag force (N/m ³)	σ	Solid pseudo-phase
<i>g</i>	Gravitational acceleration [m/s ²]	τ_i	Solid stress strain-tensor (N/m ³)
<i>G(ε_β)</i>	Modulus of elasticity	ψ	Any field variable

G_0	Normalizing units factor	<i>Super/Subscripts and Averages</i>	
$H_{\sigma,0}$	Static bed height (mm)	cone	Relative to the cone section in the spouted bed
$K_{\sigma\beta}$	Multiphase interaction coefficient	cylinder	Relative to the cylinder section in the spouted bed
L_C	Column length (mm)	CFD	Model prediction
MSD	Mean Squared Deviation	EXP	Experimentally determined quantity
n	Total number of sample points	eff	Effective property
P	Pressure (Pa)	ms	Minimum spouting
r	Radial direction	0	Initial conditions
R_C	Column radius (m)	total	Total measuring time
Re_{mix}	Effective mixture Reynolds number	<i>Average Quantities</i>	
$SD_{\psi,t}$	Standard deviation	$\langle \rangle$	Average quantity
t	Time (s)	$\langle \rangle_t$	Time-averaged quantity
V_i	Superficial velocity of phase i (m/s)	$\langle \rangle_{\theta}$	Azimuthally averaged quantity
\mathbf{v}_i	Superficial velocity vector of phase i (m/s)	$\langle \rangle_{\theta,t}$	Azimuthally and time-averaged quantity
\mathbf{v}_{slip}	Slip velocity (m/s)		
$v_{i,j}$	j component of the superficial velocity vector of phase i (m/s)		
z	Axial direction		

References

- Mathur, K.B.; Epstein, N. Dynamics of spouted beds. *Adv. Chem. Eng.* **1974**, *9*, 111–191. [[CrossRef](#)]
- Mathur, K.B.; Gishler, P.E. A technique for contacting gases with coarse solid particles. *AIChE J.* **1955**, *1*, 157–164. [[CrossRef](#)]
- Olazar, M.; Álvarez, S.; Aguado, R.; José, M.S. Spouted bed reactors. *Chem. Eng. Technol.* **2003**, *26*, 845–852. [[CrossRef](#)]
- Cortazar, M.; Lopez, G.; Alvarez, J.; Amutio, M.; Bilbao, J.; Olazar, M. Advantages of confining the fountain in a conical spouted bed reactor for biomass steam gasification. *Energy* **2018**, *153*, 455–463. [[CrossRef](#)]
- Aguado, R.; Saldarriaga, J.F.; Atxutegi, A.; Bilbao, J.; Olazar, M. Influence of the kinetic scheme and heat balance on the modelling of biomass combustion in a conical spouted bed. *Energy* **2019**, *175*, 758–767. [[CrossRef](#)]
- Olazar, M.; Jose, M.J.S.; Aguayo, A.; Arandes, J.M.; Bilbao, J. Stable operation conditions for gas-solid contact regimes in conical spouted beds. *Ind. Eng. Chem. Res.* **1992**, *31*, 1784–1792. [[CrossRef](#)]
- Gryczka, O.; Heinrich, S.; Miteva, V.; Deen, N.G.; Kuipers, J.; Jacob, M.; Mörl, L. Characterization of the pneumatic behavior of a novel spouted bed apparatus with two adjustable gas inlets. *Chem. Eng. Sci.* **2008**, *63*, 791–814. [[CrossRef](#)]
- Lan, X.; Xu, C.; Gao, J.; Al-Dahhan, M. Influence of solid-phase wall boundary condition on CFD simulation of spouted beds. *Chem. Eng. Sci.* **2012**, *69*, 419–430. [[CrossRef](#)]
- He, Y.-L.; Lim, C.; Grace, J. Scale-up studies of spouted beds. *Chem. Eng. Sci.* **1997**, *52*, 329–339. [[CrossRef](#)]
- Al-Juwaya, T.; Ali, N.; Al-Dahhan, M. Investigation of cross-sectional gas-solid distributions in spouted beds using advanced non-invasive gamma-ray computed tomography (CT). *Exp. Therm. Fluid Sci.* **2017**, *86*, 37–53. [[CrossRef](#)]
- Ali, N.; Al-Juwaya, T.; Al-Dahhan, M. Demonstrating the non-similarity in local holdups of spouted beds obtained by CT with scale-up methodology based on dimensionless groups. *Chem. Eng. Res. Des.* **2016**, *114*, 129–141. [[CrossRef](#)]
- Ali, N.; Al-Juwaya, T.; Al-Dahhan, M. An advanced evaluation of the mechanistic scale-up methodology of gas–solid spouted beds using radioactive particle tracking. *Particuology* **2017**, *34*, 48–60. [[CrossRef](#)]
- Ali, N.; Al-Juwaya, T.; Al-Dahhan, M. An advanced evaluation of spouted beds scale-up for coating TRISO nuclear fuel particles using Radioactive Particle Tracking (RPT). *Exp. Therm. Fluid Sci.* **2017**, *80*, 90–104. [[CrossRef](#)]
- Aradhya, S.; Taofeeq, H.; Al-Dahhan, M. A new mechanistic scale-up methodology for gas-solid spouted beds. *Chem. Eng. Process. Process. Intensif.* **2016**, *110*, 146–159. [[CrossRef](#)]
- Aradhya, S.; Taofeeq, H.; Al-Dahhan, M. Evaluation of the dimensionless groups based scale-up of gas-solid spouted beds. *Int. J. Multiph. Flow* **2017**, *94*, 209–218. [[CrossRef](#)]

16. Schillinger, F.; Schildhauer, T.; Maurer, S.; Wagner, E.; Mudde, R.; Van Ommen, J.R. Generation and evaluation of an artificial optical signal based on X-ray measurements for bubble characterization in fluidized beds with vertical internals. *Int. J. Multiph. Flow* **2018**, *107*, 16–32. [[CrossRef](#)]
17. Santos, D.; Alves, G.C.; Duarte, C.R.; Barrozo, M.A. Disturbances in the hydrodynamic behavior of a spouted bed caused by an optical fiber probe: Experimental and CFD study. *Ind. Eng. Chem. Res.* **2012**, *51*, 3801–3810. [[CrossRef](#)]
18. Ali, N.; Aljuwaya, T.; Al-Dahhan, M. Evaluating the new mechanistic scale-up methodology of gas—Solid spouted beds using gamma ray computed tomography (CT). *Exp. Therm. Fluid Sci.* **2019**, *104*, 186–198. [[CrossRef](#)]
19. Zhong, H.; Zhang, J.; Liang, S.; Zhu, Y. Two-fluid model with variable particle–particle restitution coefficient: Application to the simulation of FCC riser reactor. *Part. Sci. Technol.* **2020**, *38*, 549–558. [[CrossRef](#)]
20. Zhonghua, W.; Mujumdar, A.S. CFD modeling of the gas—Particle flow behavior in spouted beds. *Powder Technol.* **2008**, *183*, 260–272. [[CrossRef](#)]
21. Hosseini, S.H.; Ahmadi, G.; Olazar, M. CFD simulation of cylindrical spouted beds by the kinetic theory of granular flow. *Powder Technol.* **2013**, *246*, 303–316. [[CrossRef](#)]
22. Moliner, C.; Marchelli, F.; Spanachi, N.; Martínez-Felipe, A.; Bosio, B.; Arato, E. CFD simulation of a spouted bed: Comparison between the Discrete Element Method (DEM) and the Two Fluid Model (TFM). *Chem. Eng. J.* **2019**, *377*, 120466. [[CrossRef](#)]
23. Lüle, S.Ş.; Çolak, Ü.; Koksall, M.; Kulah, G. CFD simulations of hydrodynamics of conical spouted bed nuclear fuel coatiers. *Chem. Vap. Depos.* **2015**, *21*, 122–132. [[CrossRef](#)]
24. Du, W.; Bao, X.; Xu, J.; Wei, W. Computational Fluid Dynamics (CFD) modeling of spouted bed: Assessment of drag coefficient correlations. *Chem. Eng. Sci.* **2006**, *61*, 1401–1420. [[CrossRef](#)]
25. Liu, M.; Chen, Z.; Chen, M.; Shao, Y.; Liu, B.; Tang, Y. Scale-up strategy study of coating furnace for TRISO particle fabrication based on numerical simulations. *Nucl. Eng. Des.* **2020**, *357*, 110413. [[CrossRef](#)]
26. Liu, M.; Wen, Y.; Liu, R.; Liu, B.; Shao, Y. Investigation of fluidization behavior of high density particle in spouted bed using CFD–DEM coupling method. *Powder Technol.* **2015**, *280*, 72–82. [[CrossRef](#)]
27. Marchelli, F.; Moliner, C.; Curti, M.; Bosio, B.; Arato, E. CFD-DEM simulations of a continuous square-based spouted bed and evaluation of the solids residence time distribution. *Powder Technol.* **2020**, *366*, 840–858. [[CrossRef](#)]
28. Yang, S.; Fan, F.; Wei, Y.; Hu, J.; Wang, H.; Wu, S. Three-dimensional MP-PIC simulation of the steam gasification of biomass in a spouted bed gasifier. *Energy Convers. Manag.* **2020**, *210*, 112689. [[CrossRef](#)]
29. Tsuo, Y.P.; Gidaspow, D. Computation of flow patterns in circulating fluidized beds. *AIChE J.* **1990**, *36*, 885–896. [[CrossRef](#)]
30. Chapman, S.; Cowling, T. *The Mathematical Theory of Non-Uniform Gases*, 3rd ed.; Cambridge Math: Cambridge, UK, 1970.
31. Ding, J.; Gidaspow, D. A bubbling fluidization model using kinetic theory of granular flow. *AIChE J.* **1990**, *36*, 523–538. [[CrossRef](#)]
32. Van Wachem, B.; Almstedt, A. Methods for multiphase computational fluid dynamics. *Chem. Eng. J.* **2003**, *96*, 81–98. [[CrossRef](#)]
33. Ferraro, V.C.A.; Chapman, S.; Cowling, T.G. The mathematical theory of non-uniform gases. An account of the kinetic theory of viscosity, thermal conduction, and diffusion in gases. *Math. Gaz.* **1954**, *38*, 63. [[CrossRef](#)]
34. Verma, V.; Li, T.; Dietiker, J.-F.; Rogers, W.A. Hydrodynamics of gas—Solids flow in a bubbling fluidized bed with immersed vertical U-tube banks. *Chem. Eng. J.* **2016**, *287*, 727–743. [[CrossRef](#)]
35. Acosta-Iborra, A.; Sobrino, C.; Hernández-Jiménez, F.; De Vega, M. Experimental and computational study on the bubble behavior in a 3-D fluidized bed. *Chem. Eng. Sci.* **2011**, *66*, 3499–3512. [[CrossRef](#)]
36. Moliner, C.; Marchelli, F.; Bosio, B.; Arato, E. Modelling of spouted and spout-fluid beds: Key for their successful scale up. *Energies* **2017**, *10*, 1729. [[CrossRef](#)]
37. Massimilla, L.; Donsi', G.; Zucchini, C. The structure of bubble-free gas fluidized beds of fine fluid cracking catalyst particles. *Chem. Eng. Sci.* **1972**, *27*, 2005–2015. [[CrossRef](#)]
38. Donsi', G.; Massimilla, L. Bubble-free expansion of gas-fluidized beds of fine particles. *AIChE J.* **1973**, *19*, 1104–1110. [[CrossRef](#)]
39. Baerns, M. Effect of interparticle adhesive forces on fluidization of fine particles. *Ind. Eng. Chem. Fundam.* **1966**, *5*, 508–516. [[CrossRef](#)]

40. Rietema, K.; Cottaar, E.; Piepers, H. The effects of interparticle forces on the stability of gas-fluidized beds—II. Theoretical derivation of bed elasticity on the basis of van der Waals forces between powder particles. *Chem. Eng. Sci.* **1993**, *48*, 1687–1697. [[CrossRef](#)]
41. Rietema, K.; Piepers, H. The effect of interparticle forces on the stability of gas-fluidized beds—I. Experimental evidence. *Chem. Eng. Sci.* **1990**, *45*, 1627–1639. [[CrossRef](#)]
42. Etehadieh, B.; Gidaspow, D.; Lyczkowski, R.W. Hydrodynamics of fluidization in a semicircular bed with a jet. *AIChE J.* **1984**, *30*, 529–536. [[CrossRef](#)]
43. Bouillard, J.X.; Lyczkowski, R.W.; Gidaspow, D. Porosity distributions in a fluidized bed with an immersed obstacle. *AIChE J.* **1989**, *35*, 908–922. [[CrossRef](#)]
44. Gidaspow, D.; Syamlal, M. Solid-Gas Critical Flow. In *Proceedings of the American Institute of Chemical Engineers Annual Winter Meeting*; American Institute of Chemical Engineers: Chicago, WA, USA, 1985.
45. Hosseini, S.H.; Fattahi, M.; Ahmadi, G. Hydrodynamics studies of a pseudo 2D rectangular spouted bed by CFD. *Powder Technol.* **2015**, *279*, 301–309. [[CrossRef](#)]
46. Liu, G.-Q.; Li, S.; Zhao, X.-L.; Yao, Q. Experimental studies of particle flow dynamics in a two-dimensional spouted bed. *Chem. Eng. Sci.* **2008**, *63*, 1131–1141. [[CrossRef](#)]
47. Moliner, C.; Marchelli, F.; Ong, L.; Martinez-Felipe, A.; Van Der Dominic, A.; Arato, E. Sensitivity analysis and validation of a Two Fluid Method (TFM) model for a spouted bed. *Chem. Eng. Sci.* **2019**, *207*, 39–53. [[CrossRef](#)]
48. Alwan, G.M.; Aradhya, S.B.; Al-Dahhan, M.H. Study of solids and gas distribution in spouted bed operated in stable and unstable conditions. *J. Eng. Res. Appl.* **2014**, *4*, 2248–9622.
49. Uddin, M.H.; Coronella, C.J. Effects of grid size on predictions of bed expansion in bubbling fluidized beds of Geldart B particles: A generalized rule for a grid-independent solution of TFM simulations. *Particuology* **2017**, *34*, 61–69. [[CrossRef](#)]
50. Enwalds, H.; Peirano, E.; Almstedt, A. Eulerian two-phase flow theory applied to fluidization. *Int. J. Multiph. Flow* **1996**, *22*, 21–66. [[CrossRef](#)]
51. Pritchett, J.W. A numerical model of gas fluidized beds. *AIChE Symp. Ser.* **1978**, *74*, 134–148.
52. Gidaspow, D. *Multiphase Flow and Fluidization*; Elsevier BV: Amsterdam, The Netherlands, 1994.
53. Kaae, J. Relations between the structure and the mechanical properties of fluidized-bed pyrolytic carbons. *Carbon* **1971**, *9*, 291–299. [[CrossRef](#)]
54. Orr, C., Jr. *Particulate Technology*; McMillan: New York, NY, USA, 1966.
55. De Klerk, A. Voidage variation in packed beds at small column to particle diameter ratio. *AIChE J.* **2003**, *49*, 2022–2029. [[CrossRef](#)]
56. Crowe, C.; Schwarzkopf, J.; Sommerfeld, M.; Tsuji, Y. *Multiphase Flows with Droplets and Particles*, 2nd ed.; CRC Press: New York, NY, USA, 2011.
57. Syamlal, M.; O'Brien, T. Computer simulation of bubbles in a fluidized bed. *AIChE Symp. Ser.* **1989**, *85*, 22–31.
58. Ishii, M.; Zuber, N. Drag coefficient and relative velocity in bubbly, droplet or particulate flows. *AIChE J.* **1979**, *25*, 843–855. [[CrossRef](#)]
59. Schiller, L. A drag coefficient correlation. *Zeit. Ver. Deutsch. Ing.* **1933**, *77*, 318–320.
60. José, M.S.; Olazar, M.; Aguado, R.; Bilbao, J. Influence of the conical section geometry on the hydrodynamics of shallow spouted beds. *Chem. Eng. J. Biochem. Eng. J.* **1996**, *62*, 113–120. [[CrossRef](#)]
61. Varma, R.; Bhusarapu, S.; O'Sullivan, J.A.; Al-Dahhan, M. A comparison of alternating minimization and expectation maximization algorithms for single source gamma ray tomography. *Meas. Sci. Technol.* **2007**, *19*, 15506. [[CrossRef](#)]
62. Efhaima, A.; Al-Dahhan, M. Local time-averaged gas holdup in fluidized bed reactor using gamma ray computed tomography technique (CT). *Int. J. Ind. Chem.* **2015**, *6*, 143–152. [[CrossRef](#)]
63. Al Falahi, F.; Al-Dahhan, M. Experimental investigation of the pebble bed structure by using gamma ray tomography. *Nucl. Eng. Des.* **2016**, *310*, 231–246. [[CrossRef](#)]

